Massively parallelized molecular force manipulation with on demand thermal and optical control

Hanquan Su[1,4] Joshua M. Brockman[2,4] Yuxin Duan[1,4] Navoneel Sen[3] Hemani Chhabra[3] Alisina Bazrafshan[1] Aaron T. Blanchard[2] Travis Meyer[2] Brooke Andrews[1] Jonathan P.K. Doye[3] Yonggang Ke[1,2] R. Brian Dyer[1] Khalid Salaita[1,2,*]

[1]Department of Chemistry, Emory University, Atlanta, Georgia, 30322, United States. [2]Wallace H. Coulter Department of Biomedical Engineering, Georgia Institute of Technology and Emory University, Atlanta, Georgia, 30322, United States. [3]Physical and Theoretical Chemistry Laboratory, Department of Chemistry, University of Oxford, South Parks Road, Oxford OX1 3QZ, United Kingdom. [4]These authors contributed equally to this work.

*Correspondence should be addressed to K.S. (k.salaita@emory.edu)

ABSTRACT: In single-molecule force spectroscopy (SMFS), a tethered molecule is stretched using a specialized instrument to study how macromolecules extend under force. One problem in SMFS is the serial and slow nature of the measurements; performed one molecule at a time. To address this long-standing challenge, we report on the origami-polymer force clamp (OPFC) which enables parallelized manipulation of the mechanical forces experienced by molecules without the need for dedicated SMFS instruments or surface tethering. The OPFC positions target molecules between a rigid nanoscale DNA origami beam and a responsive polymer particle that shrinks on demand. As a proof-of-concept we record the steady state and time-resolved mechanical unfolding dynamics of DNA hairpins using the fluorescence signal from ensembles of molecules and confirm our conclusion using modeling.

INTRODUCTION

High precision techniques that can trap and apply forces to single molecules, such as atomic force microscopy (AFM)[1-2], optical tweezers[3-4], and the biomembrane force probe[5-6] have defined our understanding of how molecules respond to applied mechanical forces. These techniques have led to fundamental understanding of many processes, ranging from mechanotransduction of cell adhesion receptors[7-8] to DNA replication[9], DNA-protein interaction[10], and enzymatic reaction mechanisms[11-12]. However, single-molecule methods have limitations and fail to provide the chemical details of the dynamic changes that occur in the target molecule as it experiences an external force. One major reason for these limitations is the low throughput of SMFS[11]. Chemical analysis generally requires greater than pM concentrations which is not compatible with SMFS. It would be highly desirable to obtain the chemical spectra of the molecules experiencing forces using methods such as FT-IR, fluorescence and Raman spectroscopy, as these methods allow one to characterize the conformational changes that accompany different states and functions of proteins and nucleic acids[13-16]. One potential solution to this challenge is to parallelize SMFS. Examples of this strategy include evanescent optical waveguides[17], acoustic force spectroscopy (AFS)[18] and centrifuge force microscopy[19], which apply an external force to many molecules in parallel. These methods have shown success but are still limited in throughput as the maximum number of molecules manipulated is $\sim 10^3$. Recent work by Liedl and colleagues[20-21] exceeded this throughput limit by using a DNA origami bracket-shaped structure to clamp target molecules with constant force. However, the DNA origami clamp must be folded in a "tensed" state, and as such the force is static and cannot be synchronized or pulsed to observe the dynamic conformation changes of target molecules. A shear-flow based method recently reported by Mao and colleagues demonstrated ensemble unfolding of DNA. The shear flow generated by a homogenizer tip could unfold macromolecules over $\sim$10 min timescales[22]. Nonetheless, a method that enables rapid on-demand mechanical unfolding of ensembles of target molecules is needed for time-resolved chemical measurements.

A solution to this dilemma is to further parallelize force manipulation by many orders of magnitude and to synchronize the application of force to allow for analysis using time-resolved spectroscopy. Such methods are commonly used to study the conformational dynamics of ensembles of molecules by collecting spectroscopic signatures following a sudden (ns to μs) perturbation. For example, in a temperature-jump (T-jump) experiment, a pump laser pulse drives a transient increase in temperature while a second probe laser (e.g. fluorescence or IR) is used to interrogate the sample. T-jump IR and T-jump fluorescence are ideally suited to interrogate DNA hairpin and protein unfolding dynamics[23-25] as well as the motions of protein active sites[26], but these methods are rarely combined with force manipulation[27]. Indeed, no time-resolved techniques currently exist for triggered application of pN forces to ensembles of

molecules because of the inherent challenges of low throughput and low temporal resolution in conventional SMFS.

To meet this challenge, one needs to meet three design goals: 1) generating a nanoscale force actuator that functions in solution, 2) linking target molecules to this force-generating actuator via bottom-up synthesis, 3) engineering the force actuator such that it can be triggered rapidly (ns to μs) to apply pN forces, and achieving these three goals at molecular yields that allow for integration with chemical analysis tools. Here we report the development of the origami-polymer force clamp (OPFC), which provides a highly parallelized approach to mechanical spectroscopy that can be interrogated with chemical spectroscopy.

RESULTS AND DISCUSSION

Design and assembly of the origami polymer force clamp (OPFC). The key innovation satisfying the design goals outlined above is the use of a DNA origami "beam" platform, which serves as a programmable nanoscopic substrate to spatially organize target molecules and to

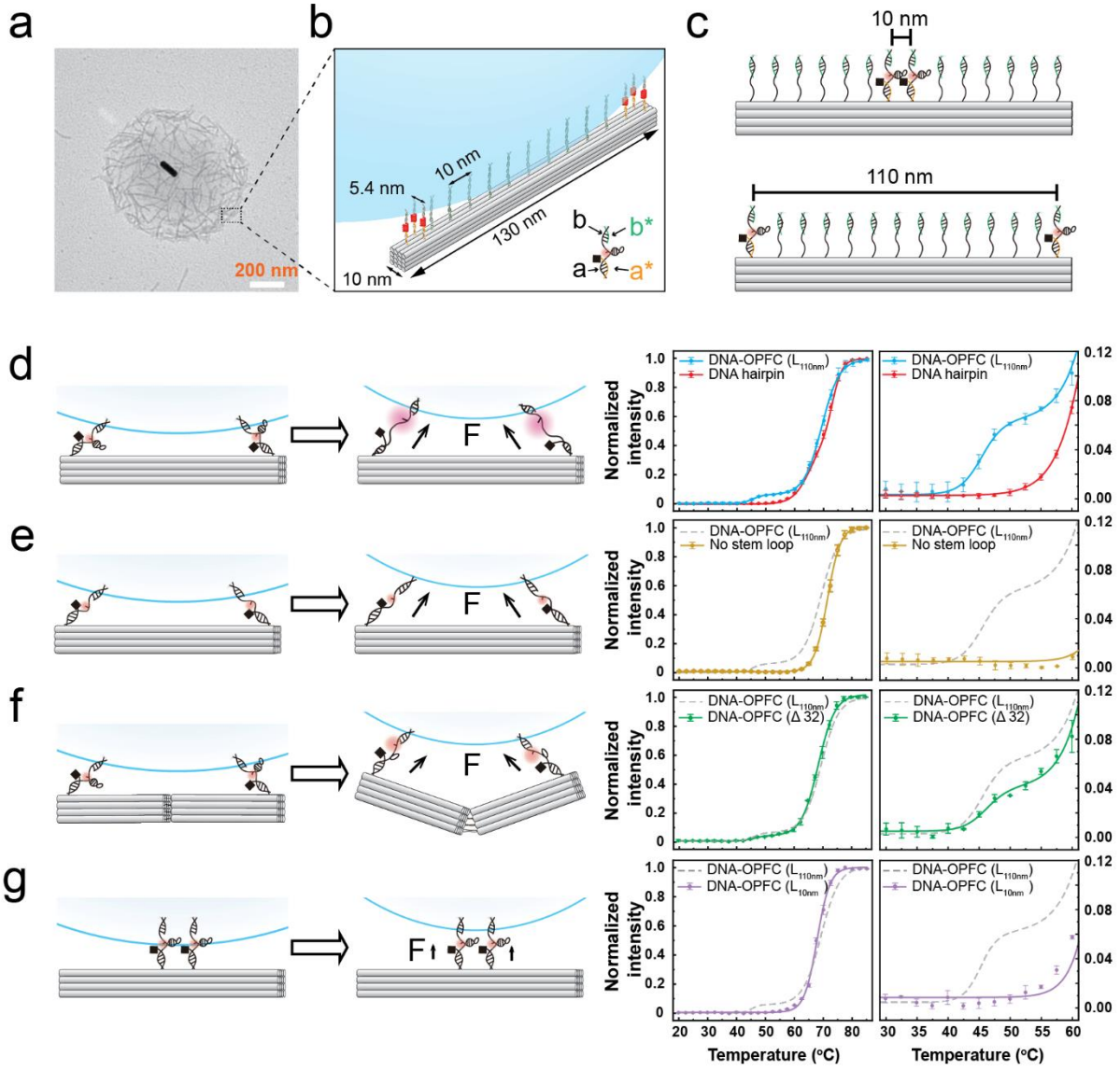

Figure 1. Origami-polymer force clamp (OPFC). (a) Representative TEM image of OPFC. (b) Schematic of OPFC showing DNA hairpins assembled between pNIPMAm polymer particle and origami 16 helix bundle (16HB) beam via a-a*/b-b* DNA hybridization. (c) Target molecules are symmetrically positioned on the beam to ensure homogeneous force magnitude, orientation, and extension. 10 crosslinks are added to increase the yield of assembly. (d) Temperature-dependent fluorescence measurements of DNA hairpins (red curve) compared to mechanical unfolding of the same hairpin using OPFC (blue curve). (e) Control structure lacking stem-loop shows no fluorescence enhancement at 45°C (yellow curve). (f) Flexible origami structure (Δ32) shows dampening of unfolding signal (green curve). (g) Force of the OPFC is tuned by changing the position of hairpins on DNA origami beam. L_{10nm} shows minimal signal enhancement compared to L_{110nm} suggesting less mechanical stress is transmitted to hairpins at the center of beam. The plot on the right in d-f highlights the inset from 30-60°C. Error bars in each curve show standard deviation of $n = 3$ experiments. The fluorescence intensity was acquired at 575 nm from temperature-dependent fluorescence spectra.

conjugate these molecules with the force-generating actuator. We chose DNA hairpins as the target because of their well-characterized unfolding trajectory and mechanical properties[28]. Our basic design of the OPFC is illustrated in **Fig. 1**. Briefly, 500 nm thermoresponsive polymer particles (pNIPMAm) were decorated with single-strand oligonucleotides (*b**) (**Fig. 1a–c**). Particle diameter is reduced by 50% upon heating above a transition temperature, thus generating a mechanical input. The DNA strands on the particle surface function as anchors to crosslink to their complementary oligonucleotides (*b*) on the rigid origami beam (**Figure S1&2**). We selected a 16-helix bundle origami beam based on modeling that factored in the tradeoff between the rigidity of the beam and its dimensions (**Note S1**). The target molecules (DNA hairpins) were modified with two orthogonal handles (*a* and *b*) such that the target molecules were immobilized site specifically between the origami beam and the polymer particle. Placing target molecules symmetrically on the 16HB is vital to ensure homogeneous mechanical perturbation of target molecules in force magnitude, orientation, and extension **(Fig. 1c**). We also placed a total of six target molecules on each origami beam to enhance the signal/noise. Engineering ten *b*-*b** crosslinks between the actuator and the origami was also important, as it boosted OPFC yield (**Figure S2**). DNA handles *a*-*a** and *b*-*b** were 18 and 21 bp in length, respectively, and designed with minimal secondary structure, high T_m, and a mechanical shearing force of ~50-60 pN[29]. Akin to the DNA handles used in optical and magnetic tweezer experiments[28, 30-31], OPFC DNA handles must withstand forces transmitted between the polymer particle and the origami platform without significant rupture (**Fig. 1c**). To assemble OPFCs, 16HB origami scaffolds (> 90% yield)[32-33] were first loaded with target molecules, and then hybridized to actuator particles to form the final structure (overnight, room temperature). Electron microscopy confirmed the successful assembly of OPFCs (**Fig. 1a**). This interaction was highly specific, as confirmed by control and *b* decorated DNA-AuNPs (**Figure S3)**. Using the extinction coefficient of the gold nanorod (AuNR) core within each OPFC ($\varepsilon_{785\,nm} = 3.7\times10^{10}$ $M^{-1}cm^{-1}$) [34] and the origami ($\varepsilon_{260\,nm} = 1\times10^{8}$ $M^{-1}cm^{-1}$)[35], we quantified the stoichiometry between origami and polymer particle = 262 ± 15 origami structures per particle (**Figure S4**). In a typical experiment, we manipulate ~10^{12} target molecules loaded in ~10^{9} OPFCs.

Ensemble unfolding of DNA hairpins using the OPFC. We next validated OPFC driven unfolding of target molecules using steady-state fluorescence measurements in bulk solution. As a proof-of-concept, we employed a stem-loop DNA hairpin that was internally labeled with a fluorophore (Cy3B) and a quencher (QSY9) that was hybridized to the anchor strands on the origami beam (Table S1-3). This fluorophore-quencher pair provided a sensitive readout of unfolding and we measured a ~730% increase in fluorescence upon heat- or duplex-induced hairpin opening (Figure S5 and S6). As a control, we measured the thermal melting profile of target DNA hairpins, which showed T_{m1} = 64 ± 0.23°C and T_{m2} = 72 ± 0.06°C using double-Boltzmann sigmoidal fitting (Fig. 1d, red curve). These T_m's correspond to the thermal melting of the hairpin stem (62°C) and arms (72°C, Figure S6). Next, we assembled the OPFC with the target hairpin and then recorded its temperature-dependent fluorescence spectra (Fig. 1d). We observed a similar spectra to the experiments using soluble hairpins but with the appearance of a new melting transition at T_m = 45°C with an amplitude of 6% of the maximum intensity (**Fig. 1d**, blue curve). This new transition shows a clear difference compared to the soluble oligonucleotides in the temperature range from 45-60°C (**Fig. 1d**). After 60°C, the soluble and OPFC anchored hairpins show nearly identical profiles. We postulate that the signal generated between 45-55°C is primarily driven by mechanical melting (unfolding) of the target DNA appropriately crosslinked between the actuator and the origami beam. Confirming that the actuator drives force generation, we found that the transition temperature of the pNIPMAm particles = 45°C with a full width at half maximum (fwhm) of 8°C, consistent with the range of temperatures showing differential unfolding between OPFC and soluble hairpin (Figure S7). To further validate that the OPFC mechanically unfolds hairpins, we performed several control experiments by taking advantage of the addressability of DNA origami design. First, we created fluorophore-quencher tagged OPFCs with the target stem-loop structure removed, and in triplicate preparations found no fluorescence enhancement at 45°C (**Fig. 1e**). This confirms the mechanical unfolding signature at 45°C is the result of DNA hairpin unfolding. We next tested the assumption that transmitting forces to the target requires a rigid beam. We removed a 32nt segment from the middle of the 16HB (Δ32) to create a flexible region at the middle of the beam (Figure S8). The number of Δ32 origami beams on the actuators remained at ~255 ± 25. Confirming our assumption, we observed a ~40% decrease in the mechanical unfolding signal compared to the parent origami structure when heated to 45°C (**Fig. 1f**). To verify that force transmission requires direct covalent coupling between the hairpin and the actuator, rather than the possibility of physical entanglement with the pNIPMAm hydrogel, we designed a zero-force control by re-positioning the hairpin to the opposite face of the origami beam which showed no notable mechanical unfolding signal in the 45-55°C window (Figure S9). Finally, we tested the force tunability of the OPFC by changing the position of hairpins on the DNA origami template. As shown in Fig. 1g, no mechanical unfolding signal was observed in the 45-55°C window when the hairpin was moved to the center of the origami beam (L_{10nm}-configuration). Taken together, the steady-state fluorescence measurements show that the OPFC transmits pN forces specifically to target molecules to drive parallelized mechanical unfolding. To the best of our knowledge, this represents the first example of a bottom-up synthesized material that can be externally triggered to apply pN forces to target molecules on demand and in bulk solution.

Time-resolved "force-jump" unfolding of DNA hairpins using OPFC. We and others previously showed that actuation of thermoresponsive nanoparticles has a time scale of τ_{50} = 10 μs (the average time to achieve 50% transition, **Table S4**)[36]. Given this fairly rapid rate of collapse, we asked whether OPFCs could enable time-resolved spectroscopic analysis of mechanical unfolding. To test this idea, we used a 1.91μm laser that triggers the synchronized collapse of actuators, thus mechanically perturbing the DNA hairpins while simultaneously recording the time-resolved fluorescence change. We dubbed this process as "force-jump" or F-

jump in analogy to the T-jump since our approach enables time-resolved spectroscopic analysis following a force pump of target molecules. Note that in our work the term "F-jump" represents an ensemble relaxation method that complements the "single molecule force-jump" optical tweezer technique introduced by Tinoco and Bustamante[37]. As shown in **Fig. 2a**, the F-jump was triggered by a Q-switched Ho:YAG IR pulse that heats the local water solvent (~1 nL). In our setup, the strong IR absorbance of H_2O generates a rapid 10°C T-jump in solution (instrument response time was ~3 µs, **Figure S10**). This was confirmed by using a calibrated Rhodamine B reference sample (**Figure S10**)[38-39]. The fluorescence signal passed through a bandpass filter and was collected by a photomultiplier tube. The final signal was digitized and averaged (3000 shots) using an oscilloscope. We selected a 10°C T-jump to accommodate the 8°C FWHM of the actuator transition while also minimizing cavitation effects.

To determine the force-induced dynamics of the hairpin, we directly compared the T-jump and F-jump responses of target hairpins (**Fig. 2b**). We first measured the equilibrium thermal melting profile of the target hairpins (**Fig. 2c**). These measurements provide the fraction of unfolded hairpins as a function of temperature which is related to the K_{eq} and the ratio of the forward (k_u) and reverse (k_f) rates of unfolding (**Fig. 2c,** T_m = 62°C; **Figure S6**). Next, a conventional T-jump measurement was used to determine the absolute values of the k_u and k_f rates of unfolding as a function of temperature (**Fig. 2d**). Specifically, the rate of relaxation (k_r), which is the sum of k_u(0 pN, T) and k_f(0 pN, T), can be determined by single exponential fitting of the T-jump as a function of the final temperature of the system (**Fig. 2d**). Using the relations shown in **Fig. 2d**, we determined the k_u(0 pN, T) and plotted this as a function of 1/T to generate an Arrhenius plot (**Fig. 2e**). As expected, we found that the rate of unfolding decreased exponentially as a function of 1/T. In theory, the k_u(0 pN, T) and k_f(0 pN, T) at all temperatures can be calculated using this approach. However, because no unfolding signal was detected in the T-jump when the T_{final} = 45°C (**Fig. 2d**), we extrapolated this value from the Arrhenius plot as shown in **Fig. 2e** (k_u(0 pN,45°C) = 151 s^{-1}). Notably, when we extrapolate k_u (0 pN, 25°C) we find that it

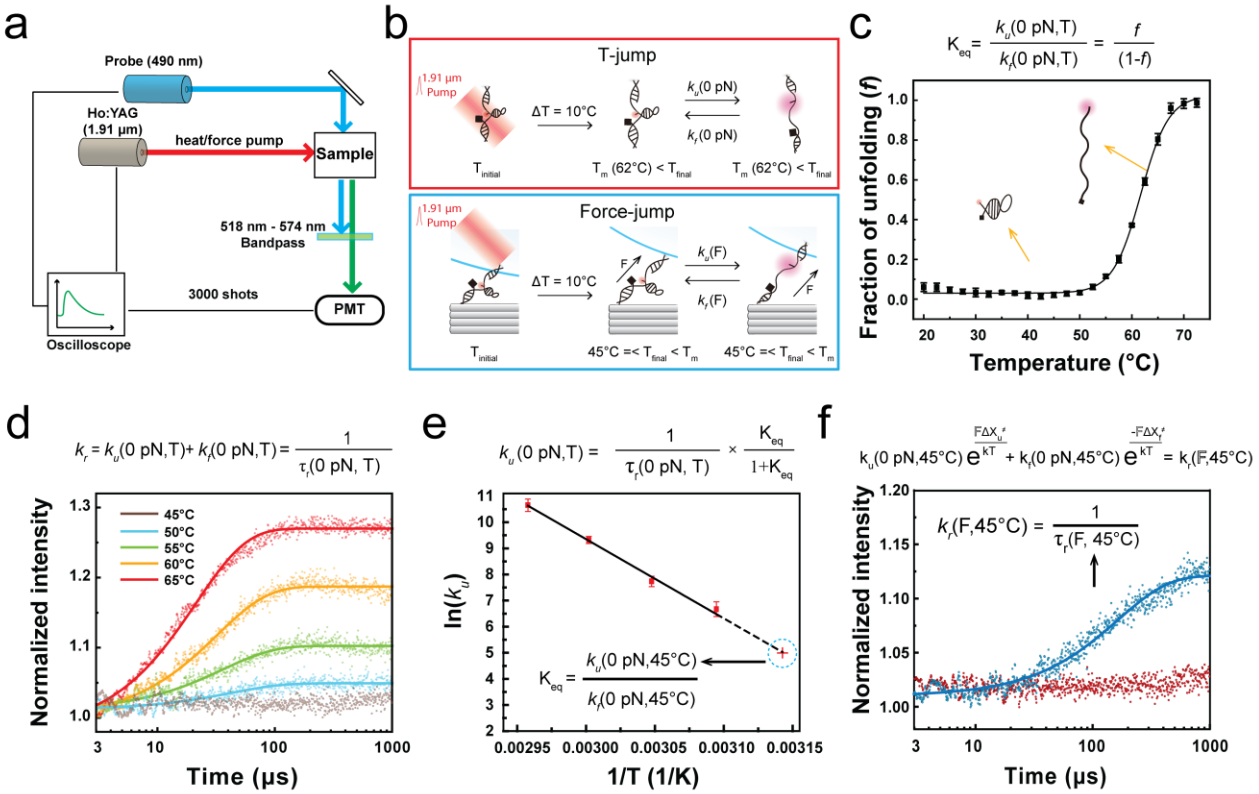

Figure 2. Time-resolved fluorescence measurement reveals DNA hairpin relaxation dynamics and magnitude of the force on the OPFC. (a) Schematic showing the experimental setup used to perform time-resolved fluorescence relaxation measurements. (b) Schematic comparing the F-jump and T-jump experiments. In the T-jump, a transient IR pump laser locally heats the sample and triggers thermal melting of the DNA hairpin. The F-jump triggers a phase transition in the OPFC which leads to mechanical melting of the DNA hairpin at the particle phase transition temperature. (c) Steady-state fluorescence measurements were used to generate a melting profile of the DNA hairpin and to determine $K_{eq} = k_u/k_f$. (d) Representative time-resolved fluorescence plots showing hairpin relaxation dynamics at different final temperatures (T_{final}). Each color denotes a different final temperature. Solid line represents a fit to the raw data. Relaxation dynamics from this conventional T-jump measurement were used to determine the relaxation rate $k_r = k_u + k_f$ of DNA melting. (e) Arrhenius plot of k_u. The k_u at 45°C was calculated by extrapolation of the Arrhenius fitting. The error bars represent the standard deviation from three independent measurements. (f) Plot comparing the F-jump (blue) and T jump (red) for the same hairpin when sample was pumped to 45°C. The solid line is a fit to the raw data.

equals 0.017 s^{-1} which is similar to reported values for stem-loop DNA hairpins with a 10-mer stem and 4 nt loop studied using optical tweezers [28]. Finally, we performed the F-jump measurement with T_{final} = 45°C because this value reaches the actuator transition (transition temperature = 45°C), while minimizing thermal unfolding of the hairpin. **Fig. 2f** shows the time-resolved fluorescence signal for the F-jump and T-jump with ΔT = 10°C (from 35 to 45°C). Spectra with greater T_{final} are shown in **Figure S11&12** for reference and show dynamics that match that reported by Ansari and others for DNA hairpins, further corroborating our results[40-41]. At T_{final} = 45°C, we observed an increase in fluorescence with a single exponential relaxation time (τ_r) = 240 ± 104 μs following the force pump (**Fig. 2f**, blue).

Importantly, performing time-resolved mechanical unfolding measurements can also be used to infer the applied force. Steady-state measurement, like the ones shown in **Fig. 1**, indicate whether the force is above a threshold value, whereas the dynamics of force-induced unfolding can provide the magnitude of the force[42]. Therefore, we next sought to estimate the magnitude of the force and the relative acceleration over thermal unfolding rates. As the Bell model predicts for an idealized two-state system[42], the k_f and k_u are exponentially modulated under tension, and one can infer the applied force by measuring the force-induced change in k_f and k_u. Using literature measurements for similar hairpin structures[28], we set the distances to the transition state, $\Delta x_u^{\neq}$ and $\Delta x_f^{\neq}$ as 4 nm and 5.1 nm. This allowed us to estimate the applied force = 3.4 ± 0.45 pN at 45°C (**Note S2)**. Interestingly, this calculated F value is lower than the calculated $F_{1/2}$ = 4.8 pN (45°C and 10 mM Mg^{2+}) for this target hairpin which is the equilibrium force that leads to a 50% probability of unfolding. This may explain the strength of the signal in **Fig. 1**. Certainly, greater forces can be obtained at higher temperatures that promote full collapse of the actuator (e.g., T_{final} ~ 55°C), but as shown in **Fig. 1** and **Fig. 2c-d**, hairpin thermal melting becomes appreciable at greater temperatures.

OxDNA simulation of the OPFC. To further validate these experiments and provide an estimate of the applied force magnitude, and to assess the effects of origami bending under the applied forces, we simulated the OPFC system with a coarse-grained DNA model (OxDNA[43-45], **Note S3**). **Fig. 3a** shows representative snapshots of each OPFC configuration before and after particle collapse (T = 40 and 55°C). The actuator-generated forces are transmitted to the origami beam through both the hairpins and linkers which cause bending of the beam toward the actuator. Although the force acting through each individual hairpin/linker is in the ~pN range (**Fig. 3b)**, the sum of all such forces accumulates and mediates beam distortion toward the particle (**Fig. 3c**). Origami bending was quantified by drawing a line through the long axis of each half-beam. As expected, hairpins and linkers were initially roughly oriented radially towards the center of the actuator. Upon actuator collapse

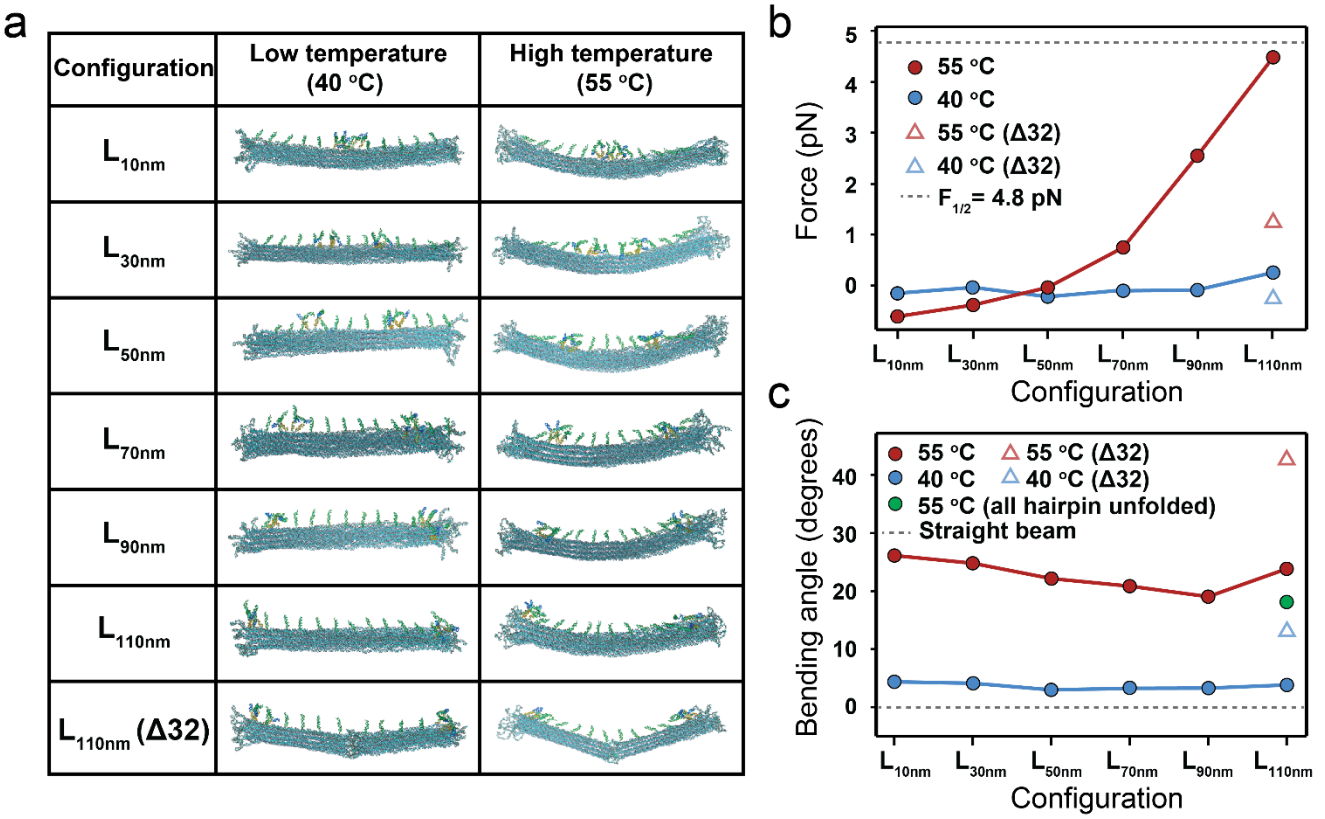

Figure 3. Coarse-grained OxDNA simulations confirm that OPFC transmits pN forces to target molecules. (a) Representative snapshots from simulations of different OPFC configurations at low and high temperature (w/ and w/o application of force). (b) Plot of average force experienced by target molecules as a function of position along origami beam at low (blue) and high (red) temperature. Results of the Δ32 beam are plotted using triangles. (c) Plot of beam bending angle as a function of hairpin positioning at low and high temperature. The green dot shows bending angle for OPFCs applying force to ssDNA presenting all T bases.

(55°C), the origami beam bends significantly as a result of the exerted forces. The average force experienced by the target molecule increased when the hairpin was positioned at the termini of the beam (from L_{10nm} to L_{110nm} **Fig. 3b**) in agreement with our experiments (**Fig. 1d-g**). In addition, the bending angle for beams decreased as we moved the hairpins from the center to the edges (L_{10nm} to $L_{90nm,}$ **Fig. 3c**). This is because hairpins have greater span than the cross-linking oligonucleotides which relieves some of the strain and reduces bending angle. Additionally, as the actuator shrinks, the hairpins and linkers in the center of the origami (red curve, L_{10nm} and L_{30nm}, **Fig. 3b**) tend to be in a state of compression rather than tension because of their proximity to the surface. Interestingly, we found that the bending angle for L_{110nm} deviates slightly from the trend and shows greater than expected bending of the origami beam. This may be because of the greater net effect of the three mainly closed hairpins compared to one linker when situated at the end. To verify the role of hairpin opening in controlling beam bending, we deliberately generated an all T base hairpin that is unable to fold. This structure showed significantly reduced bending (18°) (green dot, **Fig. 3c**), thus supporting our hypothesis. We also simulated hairpin unfolding of the flexible Δ32 origami structure. As expected, the Δ32 origami beams displayed greater bending angles and were bent at the hinge (**Fig. 3a**). Additionally, upon particle actuation, the angle of beam shifted from 13 ± 0.15° to 43 ± 0.08°. Because the Δ32 origami beam deforms to accommodate the mechanical collapse, the force experienced by the target molecules in this case was diminished (**Fig. 3b**). Taken together, OxDNA modeling aligns with the experiments and suggests that the current design of the OPFC generates ~4-5pN of force on target molecules placed at the L_{110nm} position and this value can be tuned by geometric positioning on the origami scaffold.

Our work demonstrates time-resolved chemical measurement of mechanical unfolding dynamics using a bottom-up assembled OPFC. It mirrors the capabilities of the bracket-shaped clamp system[20], providing the ability to unfold 10^{12} target molecules but with the additional ability to trigger the mechanical force on demand. It provides a novel route to bridge the gap between simulation and experimental result. Nonetheless, the OPFC approach carries several caveats. First, conventional DNA origami synthetic yields are difficult to extend beyond nM concentrations. This concentration is appropriate for fluorescence spectroscopy, but higher amount and concentrations of OPFCs are desirable for Raman, IR, and NMR measurements as well as for improving the temporal resolution of time-resolved fluorescence spectroscopy (sub 100-nsec). Further advancement in origami preparation techniques can potentially alleviate this limitation[46]. Secondly, the particle volume phase transition was triggered with an "outside-in" global heating pump which limits the OPFC collapse rate to the ~10 μs time scale. The particle collapse rate could be accelerated to τ = ~100 ns if the OPFC was heated locally "inside-out" using the gold nanorod[36]. Increasing the collapse rate by two orders of magnitude (as we have shown previously[36]), further enhances the loading rate of the OPFC. Loading forces of 1-10 pN within ~10-100 nsec provide pulling speeds that match that of the time scales of molecular dynamics (MD) simulations[47-48]. The ultrafast AFM force spectroscopy techniques developed by Perkins and others have been transformative and the OPFC may offer complementary approaches to investigating unfolding trajectories[48-49]. Greater forces could be achieved using this system as long as the origami rod deforms minimally. Previous modeling suggests that 10HB origami beam will deform if forces exceed ~60 pN at high loading rate (3.2×10^8 pN/s)[50]. To allow for greater forces and high loading rate, one would need to employ alternate origami designs with greater bending stiffness as described in reports by William Shih et al.[51] and Carlos Castro et al[52]. In the present iteration, force exertion is tied to a temperature increase that drives the phase transition of the polymer force clamp. As a general guideline, the T_m of the biomolecule should be greater than the LCST of the polymer to minimize the probability of thermal denaturation of the target. This may limit the types of biomolecules and mechanical unfolding transitions that are amenable to the OPFC strategy. Note however that the LCST can be tuned by varying the content of the thermoresponsive polymer and hence this offers a workaround for thermally sensitive target molecules[53].

CONCLUSION

In summary, our work demonstrates a novel approach for mechanically manipulating ensembles of target molecules and then to record the ensuing unfolding response using spectroscopic chemical analysis. Typically, each OPFC sample manipulates 10^{12} target molecules that are loaded and assembled using a bottom-up strategy. This level of throughput is not accessible using parallelized force spectroscopy techniques and matches the throughput of the bracket-shaped clamp approach from Liedl and colleagues[20]. Additionally, the OPFC affords the ability to separate the self-assembly step from the force loading step and to trigger the force loading at ultra-fast rates dictated by pump-probe techniques. Another key advantage of the OPFC is its amenability for integration with various spectroscopic analysis methods as well as the pump-probe family of techniques that provide a detailed readout of the molecular conformation following the mechanical pulse.

ASSOCIATED CONTENT

Supporting Information

The Supporting Information is available free of charge on the ACS Publications website.

Additional experimental details, materials, and methods, geometric analysis of DNA origami design, force estimation of hairpin unfolding, OxDNA modeling supplementary notes, OPFC synthesis, validation and TEM characterization of OPFC assembly, quantification of stoichiometry between origami and particle using UV-vis absorbance, fluorescence measurements of DNA hairpin unfolding, thermal melting of DNA hairpins, temperature-dependent DLS measurements of polymer particles, TEM characterization of flexible origami beams, zero-force control OPFC device with target hairpins, temperature calibration of T-jump experiment, replicates of T-jump and force-jump experiments, schematics of hairpin beam design, DNA and origami sequences, phase transition dynamics of thermo-responsive polymer particles, single-exponential fits of T-jump kinetics, two-way ANOVA test of temperature-dependent angle and force of the OPFC, and additional references.

AUTHOR INFORMATION

Corresponding Author

* Khalid Salaita (k.salaita@emory.edu).

Author Contributions

HS, JB, and YD contributed equally to this work. HS, JB, YD, KS designed the study. HS, JB and YD performed experiments. HS, JB, YD, NS, HC, AB analyzed data. NS, HC, ATB and JPKD performed computational modeling. YD and TM designed and synthesized DNA origami. BA and RBD assisted with T-jump and F-jump experiments and set up the instrument. HS, JB, YD, AB, ATB, YK, RBD and KS assisted with experiment design. KS, RBD, JPKD, YK supervised the study. HS, JB, YD, KS, JPKD, NS, HC, ATB wrote the manuscript

Funding Sources

National Institutes of Health grant R01GM124472
National Institutes of Health grant R01GM131099
National Science Foundation grant CHE 2004126
National Science Foundation grant DMR 1905947
National Science Foundation grant DMR-1654485
Department of Energy grant DOE DE-SC0020996
National Institutes of Health grant GM053640
Magdalen College, Oxford for the award of a Perkin Research Scholarship (HC)
EPSRC Centre for Doctoral Training, Theory and Modeling in Chemical Sciences, under grant EP/L015722/1 (HC)

Notes

The authors declare no competing financial interest.

ACKNOWLEDGMENT

K.S. would like to acknowledge support for this work through NIH R01GM124472 and R01GM131099 as well as NSF CHE 2004126 and DMR 1905947. R.B.D would like to acknowledge the support of NIH grant GM053640. Y.K. acknowledges the support of an NSF grant DMR 1654485 and a DOE grant DOE DE SC0020996. J.P.K.D acknowledges Magdalen College, Oxford for the award of a Perkin Research Scholarship (HC) and EPSRC Centre for Doctoral Training, Theory and Modeling in Chemical Sciences, under grant EP/L015722/1 (HC). This project was supported in part by the Robert P. Apkarian Integrated Electron Microscopy Core. We acknowledge the use of computational facilities provided by the University of Oxford Advanced Research Computing [doi:10.5281/zenodo.22558].

REFERENCES

1. Edwards, D. T.; Faulk, J. K.; LeBlanc, M. A.; Perkins, T. T., Force Spectroscopy with 9-us Resolution and Sub-pN Stability by Tailoring AFM Cantilever Geometry. *Biophysical journal* **2017,** *113* (12), 2595-2600.
2. Rief, M.; Gautel, M.; Oesterhelt, F.; Fernandez, J. M.; Gaub, H. E., Reversible unfolding of individual titin immunoglobulin domains by AFM. *Science* **1997,** *276* (5315), 1109-12.
3. Bustamante, C.; Bryant, Z.; Smith, S. B., Ten years of tension: single-molecule DNA mechanics. *Nature* **2003,** *421* (6921), 423-7.
4. Fazal, F. M.; Block, S. M., Optical tweezers study life under tension. *Nat Photonics* **2011,** *5*, 318-321.
5. Ju, L.; Chen, Y.; Li, K.; Yuan, Z.; Liu, B.; Jackson, S. P.; Zhu, C., Dual Biomembrane Force Probe enables single-cell mechanical analysis of signal crosstalk between multiple molecular species. *Scientific Reports* **2017,** *7* (1), 14185.
6. Liu, B.; Chen, W.; Evavold, Brian D.; Zhu, C., Accumulation of Dynamic Catch Bonds between TCR and Agonist Peptide-MHC Triggers T Cell Signaling. *Cell* **2014,** *157* (2), 357-368.
7. Seo, D.; Southard, K. M.; Kim, J. W.; Lee, H. J.; Farlow, J.; Lee, J. U.; Litt, D. B.; Haas, T.; Alivisatos, A. P.; Cheon, J.; Gartner, Z. J.; Jun, Y. W., A Mechanogenetic Toolkit for Interrogating Cell Signaling in Space and Time. *Cell* **2016,** *165* (6), 1507-1518.
8. Liu, Z.; Liu, Y.; Chang, Y.; Seyf, H. R.; Henry, A.; Mattheyses, A. L.; Yehl, K.; Zhang, Y.; Huang, Z.; Salaita, K., Nanoscale optomechanical actuators for controlling mechanotransduction in living cells. *Nat. Methods* **2016,** *13* (2), 143-6.
9. Lee, J. B.; Hite, R. K.; Hamdan, S. M.; Xie, X. S.; Richardson, C. C.; van Oijen, A. M., DNA primase acts as a molecular brake in DNA replication. *Nature* **2006,** *439* (7076), 621-4.
10. Kuhner, F.; Costa, L. T.; Bisch, P. M.; Thalhammer, S.; Heckl, W. M.; Gaub, H. E., LexA-DNA bond strength by single molecule force spectroscopy. *Biophysical journal* **2004,** *87* (4), 2683-90.
11. Dufrene, Y. F.; Evans, E.; Engel, A.; Helenius, J.; Gaub, H. E.; Muller, D. J., Five challenges to bringing single-molecule force spectroscopy into living cells. *Nat. Methods* **2011,** *8* (2), 123-7.
12. Sumbul, F.; Rico, F., Single-Molecule Force Spectroscopy: Experiments, Analysis, and Simulations. *Methods Mol Biol* **2019,** *1886*, 163-189.
13. Yang, H.; Yang, S.; Kong, J.; Dong, A.; Yu, S., Obtaining information about protein secondary structures in aqueous solution using Fourier transform IR spectroscopy. *Nat Protoc* **2015,** *10* (3), 382-96.
14. Heyduk, T.; Heyduk, E., Molecular beacons for detecting DNA binding proteins. *Nat Biotechnol* **2002,** *20* (2), 171-6.
15. Rygula, A.; Majzner, K.; Marzec, K. M.; Kaczor, A.; Pilarczyk, M.; Baranska, M., Raman spectroscopy of proteins: a review. *Journal of Raman Spectroscopy* **2013,** *44* (8), 1061-1076.
16. Becette, O. B.; Zong, G.; Chen, B.; Taiwo, K. M.; Case, D. A.; Dayie, T. K., Solution NMR readily reveals distinct structural folds and interactions in doubly ^{13}C- and ^{19}F-labeled RNAs. *Sci Adv* **2020,** *6* (41).
17. Soltani, M.; Lin, J.; Forties, R. A.; Inman, J. T.; Saraf, S. N.; Fulbright, R. M.; Lipson, M.; Wang, M. D., Nanophotonic trapping for precise manipulation of biomolecular arrays. *Nat Nanotechnol* **2014,** *9* (6), 448-52.
18. Sitters, G.; Kamsma, D.; Thalhammer, G.; Ritsch-Marte, M.; Peterman, E. J.; Wuite, G. J., Acoustic force spectroscopy. *Nat. Methods* **2015,** *12* (1), 47-50.
19. Yang, D.; Ward, A.; Halvorsen, K.; Wong, W. P., Multiplexed single-molecule force spectroscopy using a centrifuge. *Nat. Commun.* **2016,** *7*, 11026.
20. Nickels, P. C.; Wunsch, B.; Holzmeister, P.; Bae, W.; Kneer, L. M.; Grohmann, D.; Tinnefeld, P.; Liedl, T., Molecular force spectroscopy with a DNA origami-based nanoscopic force clamp. *Science* **2016,** *354* (6310), 305-307.
21. Kramm, K.; Schröder, T.; Gouge, J.; Vera, A. M.; Gupta, K.; Heiss, F. B.; Liedl, T.; Engel, C.; Berger, I.; Vannini, A.; Tinnefeld, P.; Grohmann, D., DNA origami-based single-molecule force spectroscopy elucidates RNA Polymerase III pre-initiation complex stability. *Nature Communications* **2020,** *11* (1), 2828.
22. Hu, C.; Jonchhe, S.; Pokhrel, P.; Karna, D.; Mao, H., Mechanical unfolding of ensemble biomolecular structures by shear force. *Chemical Science* **2021,** *12* (30), 10159-10164.
23. Yamamoto, K.; Mizutani, Y.; Kitagawa, T., Nanosecond Temperature Jump and Time-Resolved Raman Study of Thermal Unfolding of Ribonuclease A. *Biophysical journal* **2000,** *79* (1), 485-495.
24. Bonnet, G.; Krichevsky, O.; Libchaber, A., Kinetics of conformational fluctuations in DNA hairpin-loops. *Proc. Natl. Acad. Sci. U.S.A* **1998,** *95* (15), 8602-6.
25. Kuznetsov, S. V.; Sugimura, S.; Vivas, P.; Crothers, D. M.; Ansari, A., Direct observation of DNA bending/unbending kinetics in complex with DNA-bending protein IHF. *Proc. Natl. Acad. Sci. U.S.A* **2006,** *103* (49), 18515-20.
26. Vaughn, M. B.; Zhang, J.; Spiro, T. G.; Dyer, R. B.; Klinman, J. P., Activity-Related Microsecond Dynamics Revealed by Temperature-Jump Forster Resonance Energy Transfer Measurements on Thermophilic Alcohol Dehydrogenase. *J. Am. Chem. Soc* **2018,** *140* (3), 900-903.
27. Koirala, D.; Punnoose, J. A.; Shrestha, P.; Mao, H., Yoctoliter Thermometry for Single-Molecule Investigations: A Generic Bead-on-a-Tip Temperature-Control Module. *Angewandte Chemie International Edition* **2014,** *53* (13), 3470-3474.

28. Woodside, M. T.; Behnke-Parks, W. M.; Larizadeh, K.; Travers, K.; Herschlag, D.; Block, S. M., Nanomechanical measurements of the sequence-dependent folding landscapes of single nucleic acid hairpins. *Proc. Natl. Acad. Sci. U.S.A* **2006,** *103* (16), 6190-5.
29. Hatch, K.; Danilowicz, C.; Coljee, V.; Prentiss, M., Demonstration that the shear force required to separate short double-stranded DNA does not increase significantly with sequence length for sequences longer than 25 base pairs. *Phys Rev E Stat Nonlin Soft Matter Phys* **2008,** *78* (1 Pt 1), 011920.
30. Pfitzner, E.; Wachauf, C.; Kilchherr, F.; Pelz, B.; Shih, W. M.; Rief, M.; Dietz, H., Rigid DNA beams for high-resolution single-molecule mechanics. *Angew Chem Int Ed Engl* **2013,** *52* (30), 7766-71.
31. Cossio, P.; Hummer, G.; Szabo, A., On artifacts in single-molecule force spectroscopy. *Proc. Natl. Acad. Sci. U.S.A* **2015,** *112* (46), 14248-14253.
32. Wagenbauer, K. F.; Engelhardt, F. A. S.; Stahl, E.; Hechtl, V. K.; Stömmer, P.; Seebacher, F.; Meregalli, L.; Ketterer, P.; Gerling, T.; Dietz, H., How We Make DNA Origami. *ChemBioChem* **2017,** *18* (19), 1873-1885.
33. Bazrafshan, A.; Meyer, T. A.; Su, H.; Brockman, J. M.; Blanchard, A. T.; Piranej, S.; Duan, Y.; Ke, Y.; Salaita, K., Tunable DNA Origami Motors Translocate Ballistically Over μm Distances at nm/s Speeds. *Angewandte Chemie International Edition* **2020,** *59* (24), 9514-9521.
34. Orendorff, C. J.; Murphy, C. J., Quantitation of Metal Content in the Silver-Assisted Growth of Gold Nanorods. *The Journal of Physical Chemistry B* **2006,** *110* (9), 3990-3994.
35. Hung, A. M.; Micheel, C. M.; Bozano, L. D.; Osterbur, L. W.; Wallraff, G. M.; Cha, J. N., Large-area spatially ordered arrays of gold nanoparticles directed by lithographically confined DNA origami. *Nature Nanotechnology* **2010,** *5* (2), 121-126.
36. Zhao, J.; Su, H.; Vansuch, G. E.; Liu, Z.; Salaita, K.; Dyer, R. B., Localized Nanoscale Heating Leads to Ultrafast Hydrogel Volume-Phase Transition. *ACS Nano* **2019,** *13* (1), 515-525.
37. Li, P. T.; Collin, D.; Smith, S. B.; Bustamante, C.; Tinoco, I., Jr., Probing the mechanical folding kinetics of TAR RNA by hopping, force-jump, and force-ramp methods. *Biophysical journal* **2006,** *90* (1), 250-60.
38. Soleilhac, A.; Girod, M.; Dugourd, P.; Burdin, B.; Parvole, J.; Dugas, P. Y.; Bayard, F.; Lacote, E.; Bourgeat-Lami, E.; Antoine, R., Temperature Response of Rhodamine B-Doped Latex Particles. From Solution to Single Particles. *Langmuir : the ACS journal of surfaces and colloids* **2016,** *32* (16), 4052-8.
39. Arata, H. F.; Löw, P.; Ishizuka, K.; Bergaud, C.; Kim, B.; Noji, H.; Fujita, H., Temperature distribution measurement on microfabricated thermodevice for single biomolecular observation using fluorescent dye. *Sensors and Actuators B: Chemical* **2006,** *117* (2), 339-345.
40. Ansari, A.; Kuznetsov, S. V.; Shen, Y., Configurational diffusion down a folding funnel describes the dynamics of DNA hairpins. *Proc. Natl. Acad. Sci. U.S.A* **2001,** *98* (14), 7771-6.
41. Shen, Y.; Kuznetsov, S. V.; Ansari, A., Loop Dependence of the Dynamics of DNA Hairpins. *The Journal of Physical Chemistry B* **2001,** *105* (48), 12202-12211.
42. Bell, G. I., Models for the specific adhesion of cells to cells. *Science* **1978,** *200* (4342), 618-27.
43. Ouldridge, T. E.; Louis, A. A.; Doye, J. P. K., Structural, mechanical, and thermodynamic properties of a coarse-grained DNA model. *The Journal of chemical physics* **2011,** *134* (8), 085101.
44. Šulc, P.; Romano, F.; Ouldridge, T. E.; Rovigatti, L.; Doye, J. P. K.; Louis, A. A., Sequence-dependent thermodynamics of a coarse-grained DNA model. *The Journal of chemical physics* **2012,** *137* (13), 135101.
45. Snodin, B. E. K.; Randisi, F.; Mosayebi, M.; Šulc, P.; Schreck, J. S.; Romano, F.; Ouldridge, T. E.; Tsukanov, R.; Nir, E.; Louis, A. A.; Doye, J. P. K., Introducing improved structural properties and salt dependence into a coarse-grained model of DNA. *The Journal of chemical physics* **2015,** *142* (23), 234901.
46. Praetorius, F.; Kick, B.; Behler, K. L.; Honemann, M. N.; Weuster-Botz, D.; Dietz, H., Biotechnological mass production of DNA origami. *Nature* **2017,** *552* (7683), 84-87.
47. Rief, M.; Grubmuller, H., Force spectroscopy of single biomolecules. *Chemphyschem : a European journal of chemical physics and physical chemistry* **2002,** *3* (3), 255-61.
48. Yu, H.; Siewny, M. G.; Edwards, D. T.; Sanders, A. W.; Perkins, T. T., Hidden dynamics in the unfolding of individual bacteriorhodopsin proteins. *Science* **2017,** *355* (6328), 945-950.
49. Rico, F.; Gonzalez, L.; Casuso, I.; Puig-Vidal, M.; Scheuring, S., High-speed force spectroscopy unfolds titin at the velocity of molecular dynamics simulations. *Science* **2013,** *342* (6159), 741-3.
50. Engel, M. C.; Smith, D. M.; Jobst, M. A.; Sajfutdinow, M.; Liedl, T.; Romano, F.; Rovigatti, L.; Louis, A. A.; Doye, J. P. K., Force-Induced Unravelling of DNA Origami. *ACS Nano* **2018,** *12* (7), 6734-6747.
51. Liedl, T.; Högberg, B.; Tytell, J.; Ingber, D. E.; Shih, W. M., Self-assembly of three-dimensional prestressed tensegrity structures from DNA. *Nature Nanotechnology* **2010,** *5* (7), 520-524.
52. Castro, C. E.; Su, H.-J.; Marras, A. E.; Zhou, L.; Johnson, J., Mechanical design of DNA nanostructures. *Nanoscale* **2015,** *7* (14), 5913-5921.
53. García-Peñas, A.; Biswas, C. S.; Liang, W.; Wang, Y.; Yang, P.; Stadler, F. J., Effect of Hydrophobic Interactions on Lower Critical Solution Temperature for Poly(N-isopropylacrylamide-co-dopamine Methacrylamide) Copolymers. *Polymers* **2019,** *11* (6), 991.

Table of Contents artwork

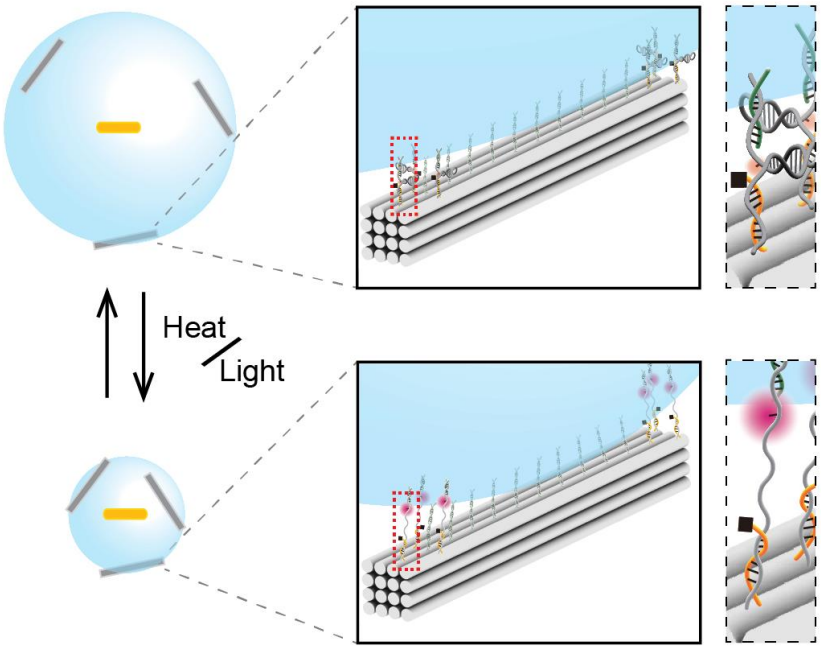
Heat
Light